Chapter 1

Introduction

Recently, numerous publications [1]-[9] have reported some low-loss dielectric and high-Q factor resonators/band-pass filters utilizing the substrate integrated waveguide (SIW) technique or electromagnetic band-gap (EBG) technique. Such a ideas of waveguides inherent the metallic waveguide, however, the solid metal walls are replaced by the via-holes array. They can be fabricated by standard printed circuit boards (PCBs) or the low temperature co-fired ceramics (LTCC) process. Similar structures realized in the LTCC process are also known as laminated waveguide and post-wall waveguide. It takes the advantages of low cost, low profile and good power handling characteristic. Besides, it can be easily integrated into microwave and millimeter wave integrated circuits. In comparison with microstrip-like structures, it has higher Q-factor. In view of the above advantages, it is a good candidate for realizing passive components in microwave and millimeter wave integrated circuits.

The cavity using the via-hole-wall technology was proposed and simulated in [1]. The three-dimensional integrated cavity resonators and filters consisting of via walls using slot excitation with a quarter open stub was successfully demonstrated. A multilayer Duroid realization of this filter was fabricated using standard printed circuit board techniques in [2]. A high-Q performance, high-port isolation and integrability to planar or 3-D circuit architectures filter, was demonstrated which was implemented by via-holes technique.

The band-pass filter under consideration in this thesis is described as follow. The band-pass filter consists of one cavity and input/output substrate integrated waveguide utilizing via-hole array to approximate the metal wall. There are two apertures

connecting the two dielectric layers, each of which couples the energy (or signal) between input (output) SIW waveguide and SIW cavity. The function of the cavity is to sever as a Fabry-Parot resonator to filter the input signal. The cavity feeding structure is a substrate integrated waveguide connecting with a taper micro-strip transition. The filter was designed at the center frequency of 5.2GHz. The bandwidth can be changed by the length of the aperture. The input and output waveguides was isolated by placing the via-hole array.

Chapter 2

The basic concept of SIW

The classical waveguide technology is still the mainstream for designing high-performance millimeter-wave systems. However, this matured scheme is not suitable for low-cost mass-production. Tedious and expensive post-fabrication tuning and assembling become a real problem for fabrication. In addition, the metallic waveguide is hard to reduce its weight and volume. Thus the substrate integrated waveguide (SIW) concept was developed and proved to be an attractive technology for low-loss, low-cost, and high-density integration of microwave and millimeter-wave components and subsystem.

The SIW technique makes it possible that a complete circuit including planar circuitry, transitions, and rectangular waveguides are fabricated in planar form using a standard printed circuit board or other planar processing techniques for widespread applications. Such a class of waveguide been proved [10] [11] to be able to preserve the well-known advantages of commonly used closed rectangular waveguide, such as high-Q factor. Besides, the substrate integrated waveguide is based on printed circuit board fabrication process; therefore, it is easy for being integrated with the micro-strip, coplanar waveguide, or the other planar circuits, to design a microwave/millimeter wave sub-system.

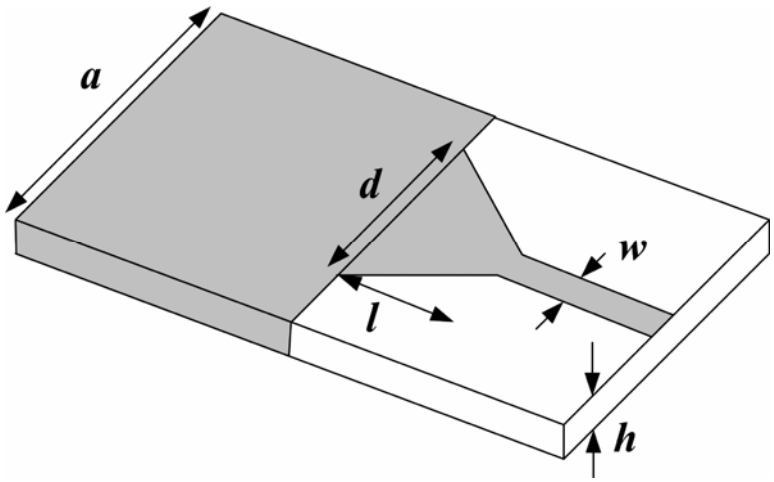

Figure 2.1 Configuration of the proposed transition of micro-strip line to rectangular waveguide on the same substrate.

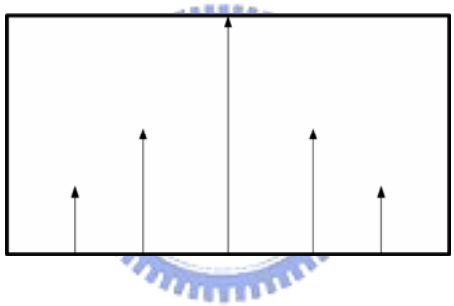

Fig. 2.2 (a) Rectangular waveguide

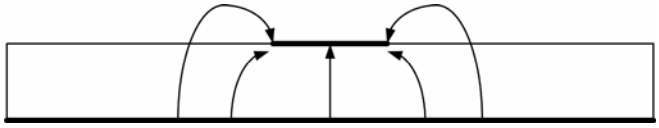

Fig. 2.2 (b) Micro-strip line

Figure 2.2 Dominant modal electric field profiles (a) in rectangular waveguide and (b) in micro-trip line

Figure 2.1 shows the proposed transition from micro-strip line to rectangular waveguide within the same dielectric substrate. The structure consists of a tapered micro-strip line section that connects a $50\,\Omega$ micro-strip line and the integrated waveguide. The tapering structure is used to transform the quasi-TEM mode of the micro-strip line into the TE_{10} mode in the waveguide. As indicated in Figure 2.2, the micro-strip line is suitably d to excite the waveguide because the electric fields of the two dissimilar structures are approximately oriented in the same direction and share the similar profile. The design criterion of such a taper transition is simple and straightforward. It is well known that the propagation constant of the TE_{10} mode is related to the width "*a*" and relative dielectric constant. Since, the height or thickness "*h*" of the waveguide is smaller compared with width "*a*". Nevertheless, reducing the height "*h*" will increase the conductor loss in both the micro-strip line and rectangular waveguide. Notice that at millimeter-wave frequencies, the waveguide section is usually compact and then the conductor loss may be maintained at a relatively low level.

A linearly tapered micro-strip is used, and this smooth transition ensures a field matching between micro-strip and rectangular waveguide over a broad band-width. The length "*l*" and width "*d*" of the taper, referring to Figure 2.1, should be modeled and optimized over the desired frequency bandwidth.

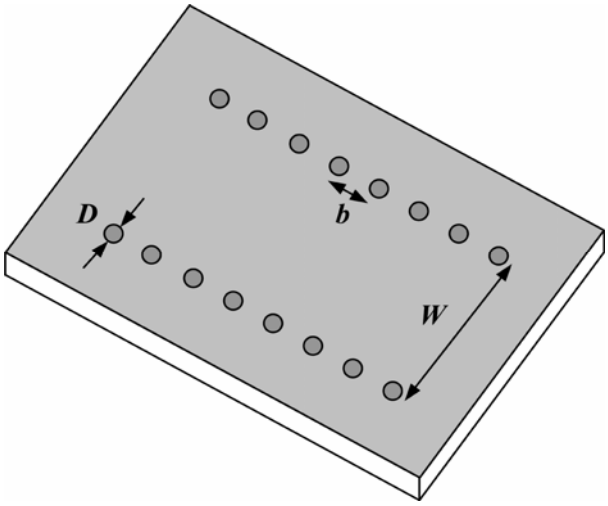

Fig. 2.3 (a)

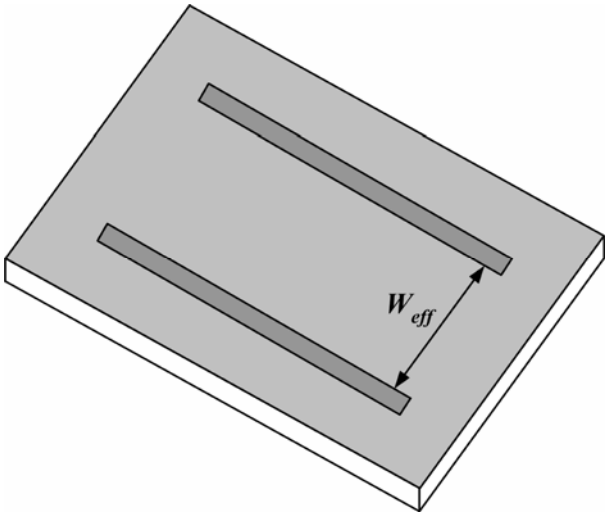

Fig. 2.3 (b)

Figure 2.3 On-substrate synthesized waveguide techniques: (a) metallic via-hole arrays and (b) metallic walls.

The sidewalls of the rectangular waveguide can be realized within the substrate using a metallic post technique (arrays of vias) or a metallic groove technique, both illustrated in Figure 2.3.

As shows in Figure 2.3, the structure parameters are given below, the diameter of the holes is denoted as D, the spacing between the holes is b, and the spacing between the two rows is W. The pitch "*b*" must be kept small to reduce the leakage loss between adjacent posts. In fact, the ratio D/b is more critical than the pitch length because the post diameter and the pitch length are interrelated as shown in [12]. Due to the synthesis, the SIW can no longer be regarded as a normal homogeneous waveguide, and it is in fact an artificial periodic waveguide. Therefore, the post diameter may significantly affect the return loss of the waveguide section in view of its input port. Two design rules related to the post diameter and pitch that are used to neglect the radiation loss are formulated in [13]. These rules have been deducted from simulation results of different SIW geometries.

$$\begin{aligned} D &< \lambda_g / 5 \\ b &\le 2D \end{aligned} \tag{2.1}$$

These two rules are sufficient but not always necessary: a diameter larger than one fifth of guided wavelength or a pitch larger than two diameters can be used but with more care. These two rules ensure that the radiation loss be kept at a negligible level.

The SIW is equivalent to a rectangular waveguide and it can be analyzed as a rectangular waveguide just by using the effective width W_{eff} of the SIW.

$$W_{eff} = W - \frac{D^2}{0.95 \times b} \tag{2.2}$$

provided that the spacing between the posts is sufficiently small.

Actually, W_{eff} is decided by three parameters, namely, *W*, *b*, and *D*. However, the modified term in (2.2) does not include the effect of *D*/*W*. when *D* increases, the small error will appear. A more accurate empirical equation is proposed here as follows:

$$W_{eff} = W - 1.08 \times \frac{D^2}{b} + 0.1 \times \frac{D^2}{W} \tag{2.3}$$

When *b*/*D* is smaller than three and *D*/*W* is smaller than 1/5, the empirical equations is very accurate.

Although the SIW structures have similar properties as the conventional rectangular waveguides, the differences between them are also obvious. First, the SIW is a sort of periodic guided-wave structure, and it may lead to an electromagnetic band-stop phenomenon. Second, the SIW structures are subject to a potential leakage problem due to the periodic gaps. Therefore, the modes or waves traveling in the SIW circuits are different from those in the normal waveguides and there exists a certain type of leakage wave.

Chapter 3

Design of the SIW cavity band-pass filter

3-1 Rectangular cavity resonator

The proposed cavity resonators are based on the theory of rectangular cavity resonators [14] and all designs and optimized with the aid of a CST Microwave Studio. The cavity resonator is built utilizing conducting planes as horizontal walls and via-hole-wall as sidewalls, as shown in Figure 3.1.

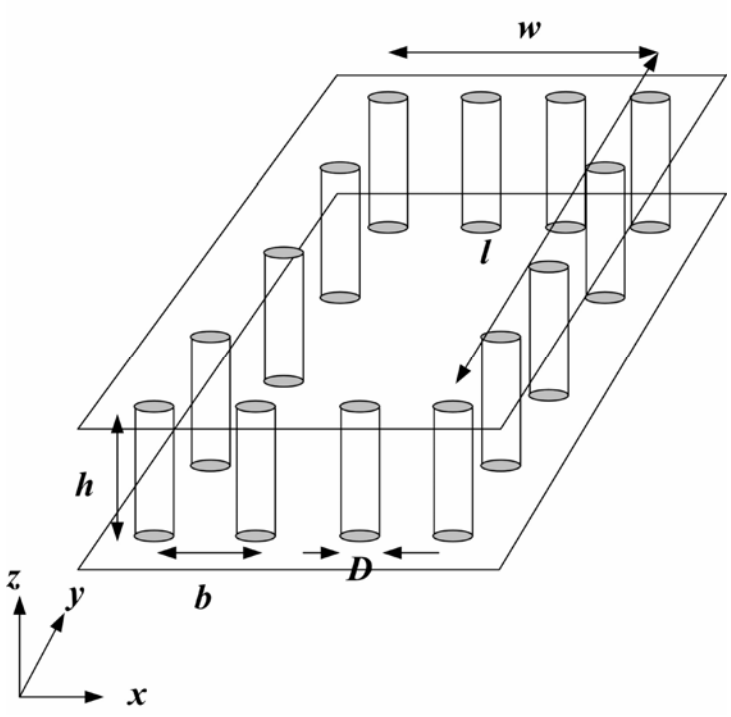

Figure 3.1 Cavity resonator utilizing via fences as sidewalls.

The diameter "*D*" and spacing "*b*" of via posts are properly chosen to prevent electromagnetic field leakage and to achieve stop-band characteristic at the desired

resonant frequency. The resonant frequency of the TM_{mnl} mode is obtained by

$$f_{res} = \frac{c}{2\pi\sqrt{\varepsilon_s}}\sqrt{\left(\frac{m\pi}{w}\right)^2 + \left(\frac{n\pi}{l}\right)^2 + \left(\frac{p\pi}{h}\right)^2} \tag{3.1}$$

Where f_{res} is the resonant frequency, c is the speed of light, ε_r is the dielectric constant, "*l*" is the length of the cavity, "*w*" is the width of the cavity, and "*h*" is the height of the cavity. Using (3.1), the initial dimensions of the cavity with perfectly conducting walls are determined for a resonant frequency of 5.2GHz for the TM_{110} dominant mode by simply indexing m=1, n=1, p=0 and optimized with a full-wave electromagnetic simulator (w=17mm, l=17mm, h=0.508mm). The design parameters of the feeding structures are then slightly modified to achieve the best performance in term of low insertion loss and accurate resonant frequency.

To decrease the metal loss and enhance the Q factor, the vertical conducting walls are replaced by a lattice of via posts. In our case, we used Cassivi's expressions [7] to get the preliminary design values, and then the final dimensions of the cavity are fine tuned with the CST microwave studio simulator. The spacing *"b"* between the via posts of the sidewalls is limited to less than half guided wavelength ($\lambda_g/2$) at the highest frequency of interest so that the radiation losses becomes negligible.

In the case of low external coupling, the unloaded Q (Q_u) is controlled by three loss mechanisms and is defined by

$$Q_u = \left(\frac{1}{Q_{cond}} + \frac{1}{Q_{dielec}} + \frac{1}{Q_{rad}}\right)^{-1} \tag{3.2}$$

Where Q_{cond}, Q_{dielec}, and Q_{rad} take into account the conductor loss from the horizontal

plates (the metal loss of the horizontal plates dominates, especially for a thin substrate such as 0.508mm), the dielectric loss from the filling substrates, and the leakage loss through the via walls, respectively. Since the gap between the via posts is less than $\lambda_g/2$ at the highest frequency of interest as mentioned, the leakage (radiation) loss can be negligible as mentioned above and the individual quantity of two other Q factors can be obtained from [15]

$$Q_{cond} = \frac{(kwl)^3 h\eta}{2\pi^2 R_m \left(2w^3 h + 2l^3 h + w^3 l + l^3 w\right)} \tag{3.3}$$

Where

w, l and h effective cavity width, length and height, respectively:

η wave impedance;

k wave number in the resonator $((2\pi f_{res}(\varepsilon_r)^{1/2})/c)$;

R_m surface resistance of the cavity ground planes $((\pi f_{res}\mu/\sigma)^{1/2})$;

$$Q_{dielec} = \frac{1}{\tan(\delta)} \tag{3.4}$$

Where tan δ is the loss tangent of the substrate.

In the chapter 4, simulation results of the SIW cavity are given. From the results, we can see that the power leakage via the gaps of the SIW cavity is much smaller than that from the conductor loss and the dielectric dissipation in the total power dissipation when certain conditions are satisfied.

3-2 The band-pass filter structure

Figure 3.2 (a)-(b) show that the top layer and bottom layer band-pass filter structure, respectively. This band-pass filter consists of two dielectric layers. The top layer contains the input and output via-hole-wall waveguides and the bottom layer contains a via-hole-wall cavity. The electromagnetic field coupling between the via-hole-wall waveguide and cavity is through the two apertures etched on the top surface of the cavity, and on the bottom surface of the waveguides, as well. The two input/output waveguides was isolated by placing the via-hole array between them. Notice that the pitch of the via-hole array separating the input and output waveguides should be kept as small as possible for preventing the direct coupling between the two waveguides. Besides, the input and output via-hole-wall waveguides are fed, respectively, by the micro-strip line with linear taper transition. The waveguide side walls or cavity walls are made from the double rows of via-wall to reduce the electromagnetic wave leakage.

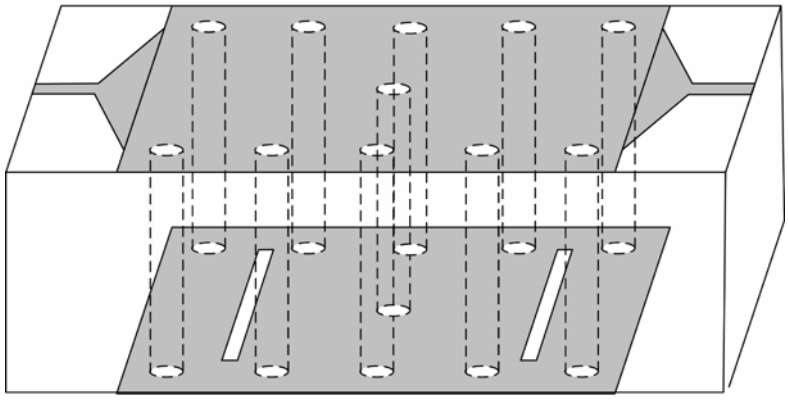

Fig. 3.2 (a)

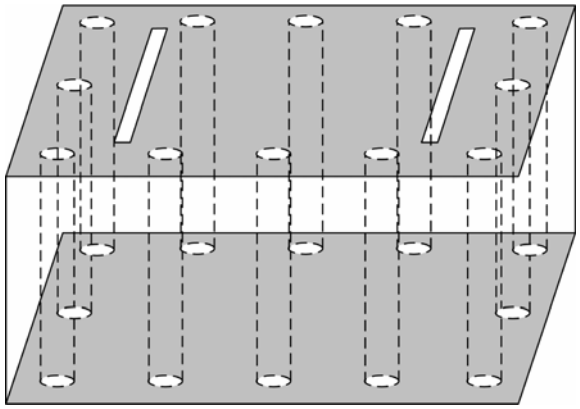

Fig. 3.2 (b)

Figure 3.2 3-D overview of band-pass filter structure (a) first layer (b) second layer

Chapter 4

Simulation and measurement results

In this thesis, we were carried out using the CST Microwave Studio for the scattering characteristics. This simulation software is base on the Finite Integration Technique (FIT) in time domain. The band-pass filter was fabricated using microwave substrate RO4003, relative dielectric constant ε_r=3.38, thickness 0.508mm, loss tangent tanδ=0.0027. The via-hole arrays were implemented using electronic plating technique. The measurement is performed using an HP8722D network analyzer.

Figure 4.1 (a)-(d) show that the parameters for the every layer structure. Their sizes were listed in the table 1. Figure 4.1 (a)-(b) depicted the top side and bottom side of the first layer for the band-pass filter structure, respectively. The top side included the input and output via-hole-wall waveguides that are fed by the micro-strip line with linear taper transition. Between the input and the output waveguide was isolated by placing the via-hole array. The bottom of the first layer etched two apertures. Figure 4.1 (c)-(d) show that the top side and bottom side of the second layer, respectively. In the resonant cavity, the top side of the second layer including two coupling apertures that the electromagnetic field coupling is taking place between the substrate integrated waveguide and the cavity resonator.

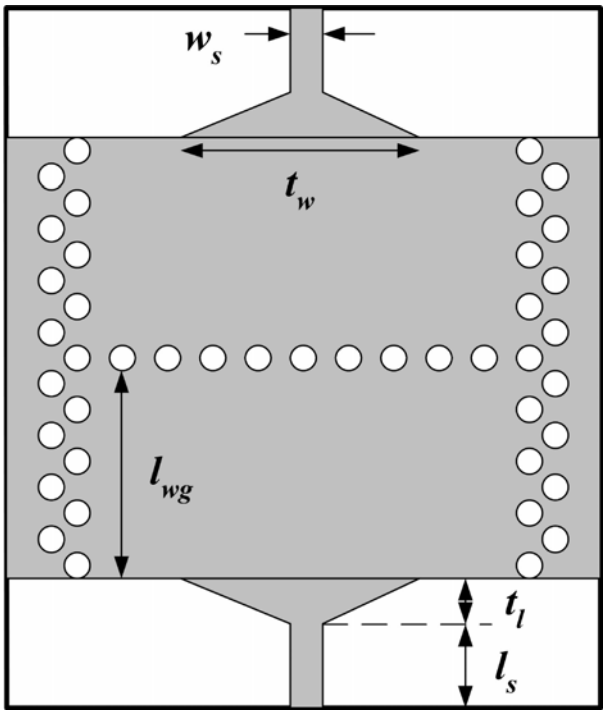

Fig. 4.1 (a)

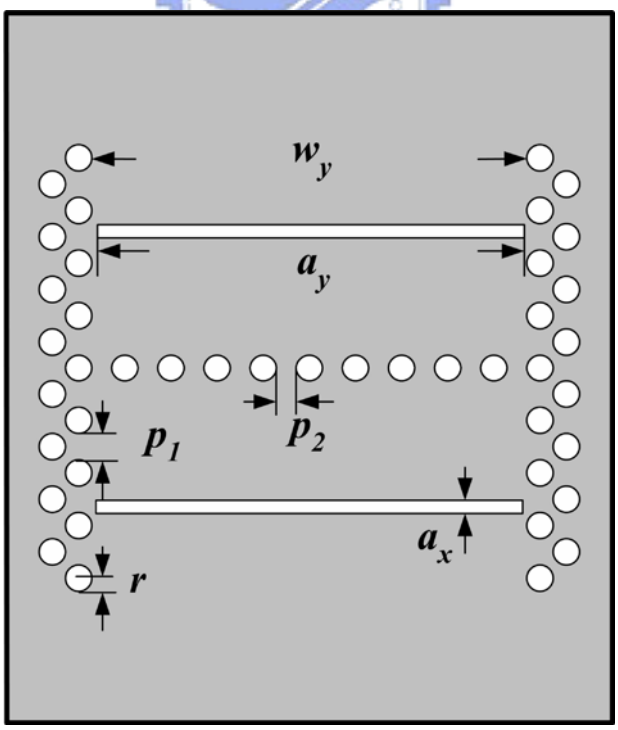

Fig. 4.1 (b)

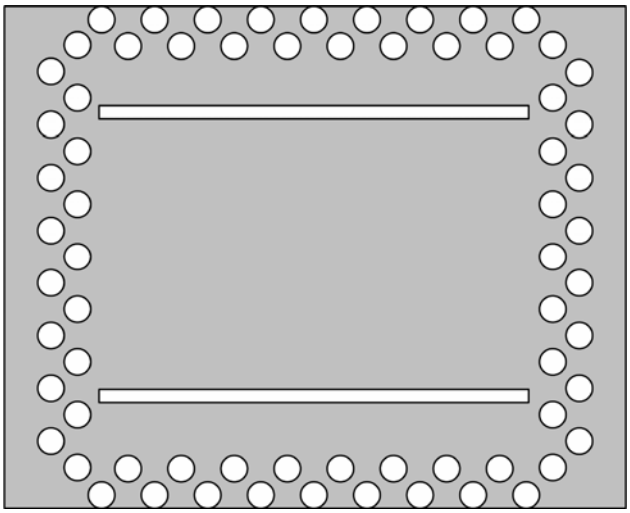

Fig. 4.1 (c)

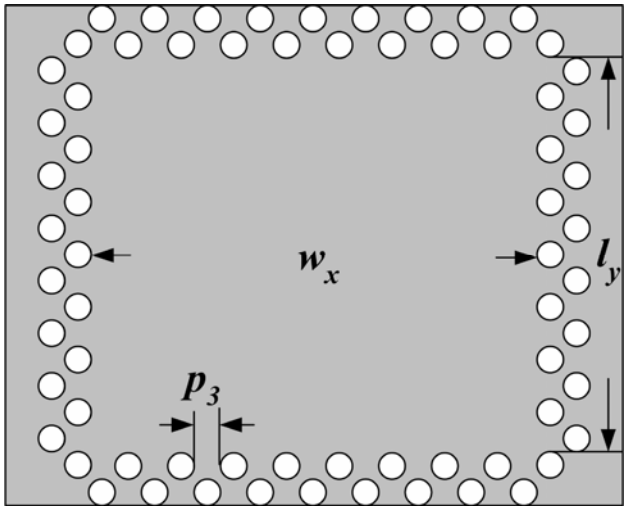

Fig 4.1 (d)

Figure 4.1 Structure configuration of the SIW band-pass filter using via-hole arrays; (a): first layer (top side) including two via-hole-wall waveguide, (b): bottom side, (c): top side of the second layer including two coupling apertures in the resonant cavity, and (d): bottom side of the resonant cavity.

radius of via hole: r	0.5 mm
width of waveguide (cavity width): w_y	17 mm
via-hole array (waveguide wall) pitch: p_1	1 mm
via-hole array (partition wall) pitch: p_2	0.55 mm
via-hole array (the second row) pitch: p_3	0.8 mm
aperture length: a_y	17 mm
aperture width: a_x	0.6 mm
input/output waveguide length: l_{wg}	7.3 mm
cavity length: w_x	17 mm
cavity length: w_y	15 mm
micro-strip line width: w_s	1.2 mm
micro-strip line length: l_s	3 mm
taper transition width: t_w	9 mm
taper transition length: t_l	1.7 mm

Table 4.1 Structure parameter

Table 4.1 indicates that the band-pass filter size. The width of the waveguide is 17 mm. The cutoff frequency f_{mn} can be easily obtained by

$$f = \frac{1}{2\pi\sqrt{\varepsilon\mu}}\sqrt{\left(\frac{m\pi}{a}\right)^2 + \left(\frac{n\pi}{b}\right)^2} \tag{4.1}$$

Where the integer *m* and *n* denote the index number along width and height direction, respectively. Since the width of the waveguide is far larger than the height. Therefore, the propagation mode is TE_{10}. Figure 4.2 shows that the cutoff frequency is 4.03 GHz by high-pass filter. The cutoff frequency is lower than that we developed pass-band frequency of the band-pass filter. The calculation of the equivalent width W_{eff} is given in Chapter 2 above, then into the (4.1) can be also calculated the cutoff frequency.

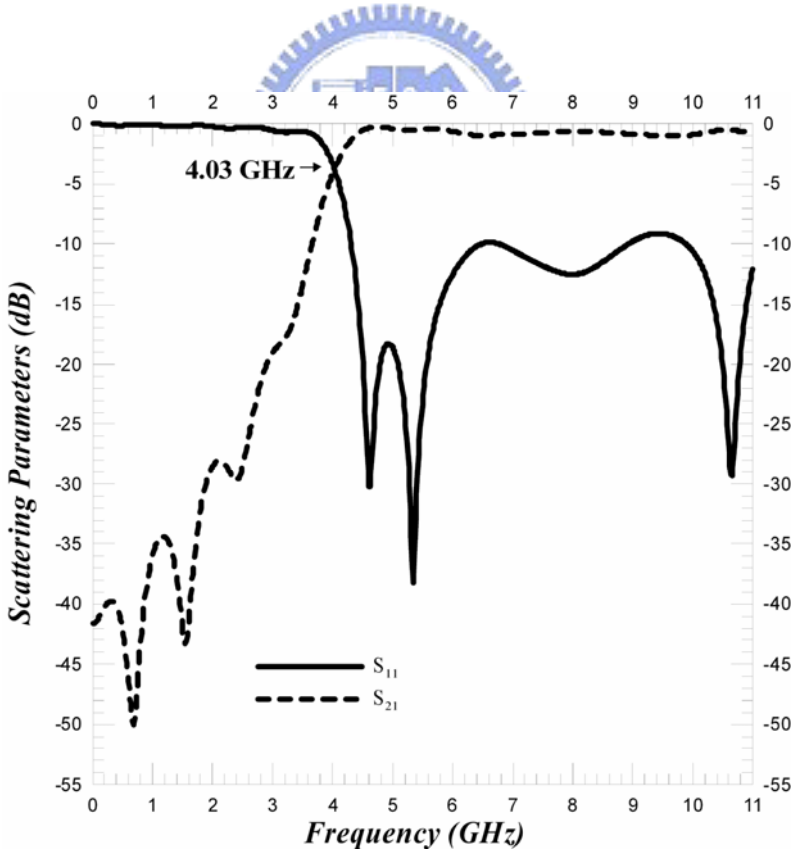

Figure 4.2 Simulated insertion loss for the substrate integrated waveguide with waveguide width 17 mm

Figure 4.3 is the simulated result of the band-pass filter with changing the length of the aperture while keeping all the other parameters. Form these figures, we found that the bandwidth of the band-pass filter can be altered by changing the length of the aperture. When the bandwidth is increasing as the aperture length is increased. It may be conjectured that due to the increase in the length of coupling aperture the coupling coefficient between the waveguide and cavity increases accordingly. The return loss and the return loss are presented in Figure 4.3 (a) and Figure 4.3 (b) respectively.

Figure 4.4 (a)-(b) show the variation of return loss and insertion loss versus frequency for various position of aperture. The positions of the two coupling aperture have to be properly designed to achieve a good performance in scattering parameters. The distance of aperture relative to the first layer centerline form 4.2 mm to 5.7 mm is shown in Figure 4.4(a) and (b). From these figures, the positions of the two coupling aperture are more close to the first layer centerline that the stop-band bandwidth will become significantly large. However, the return loss is more than -10 dB.

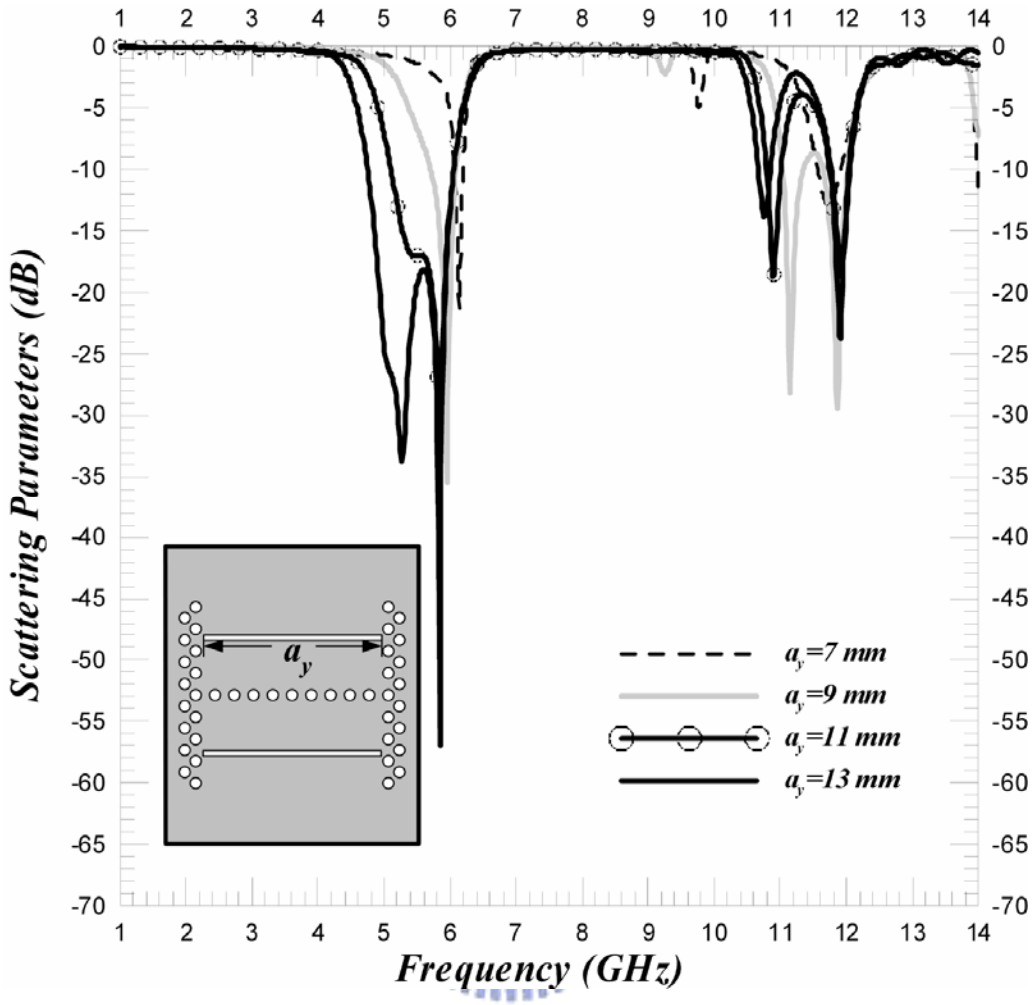
Scattering Parameters (dB)
Frequency (GHz)
a_y
a_y=7 mm
a_y=9 mm
a_y=11 mm
a_y=13 mm

Fig.4.3 (a)

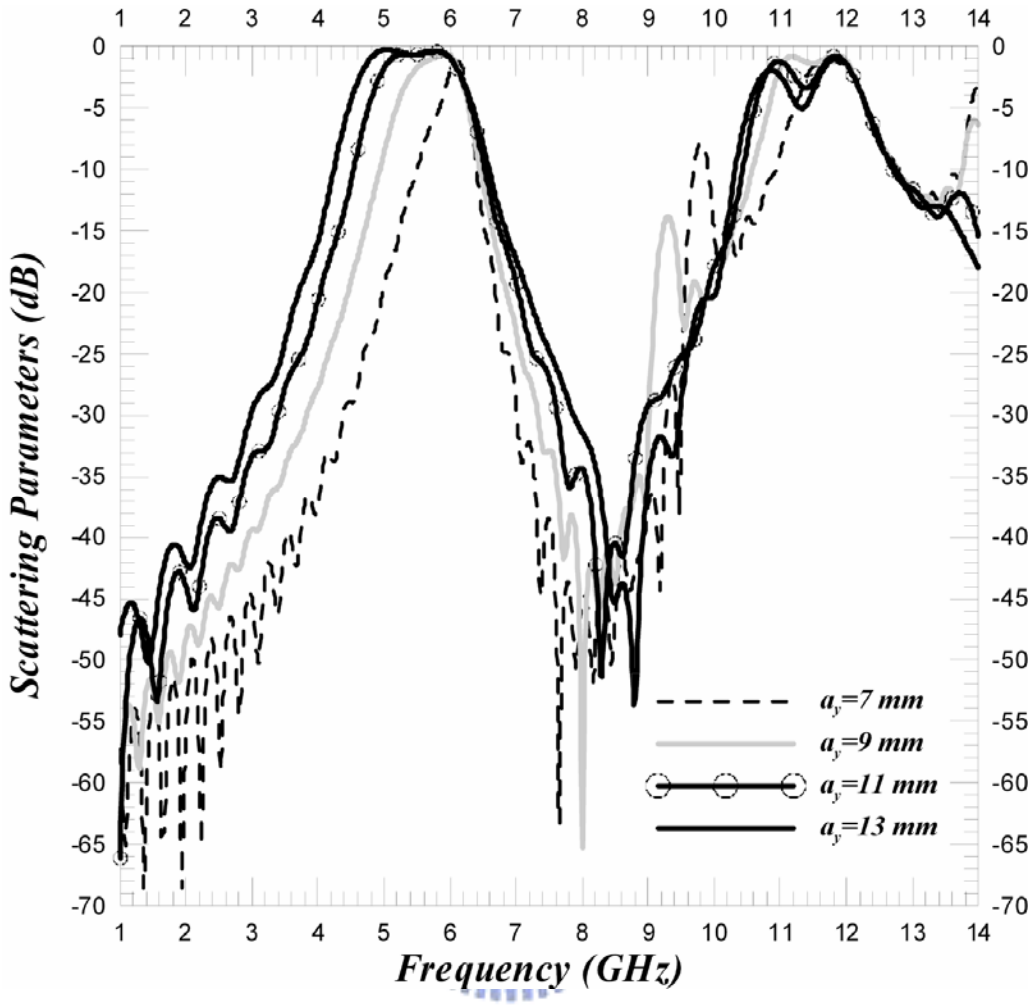

Fig 4.3 (b)

Figure 4.3 The simulation of the tunable band-pass filter with the length of aperture

(a) return loss (b) insertion loss

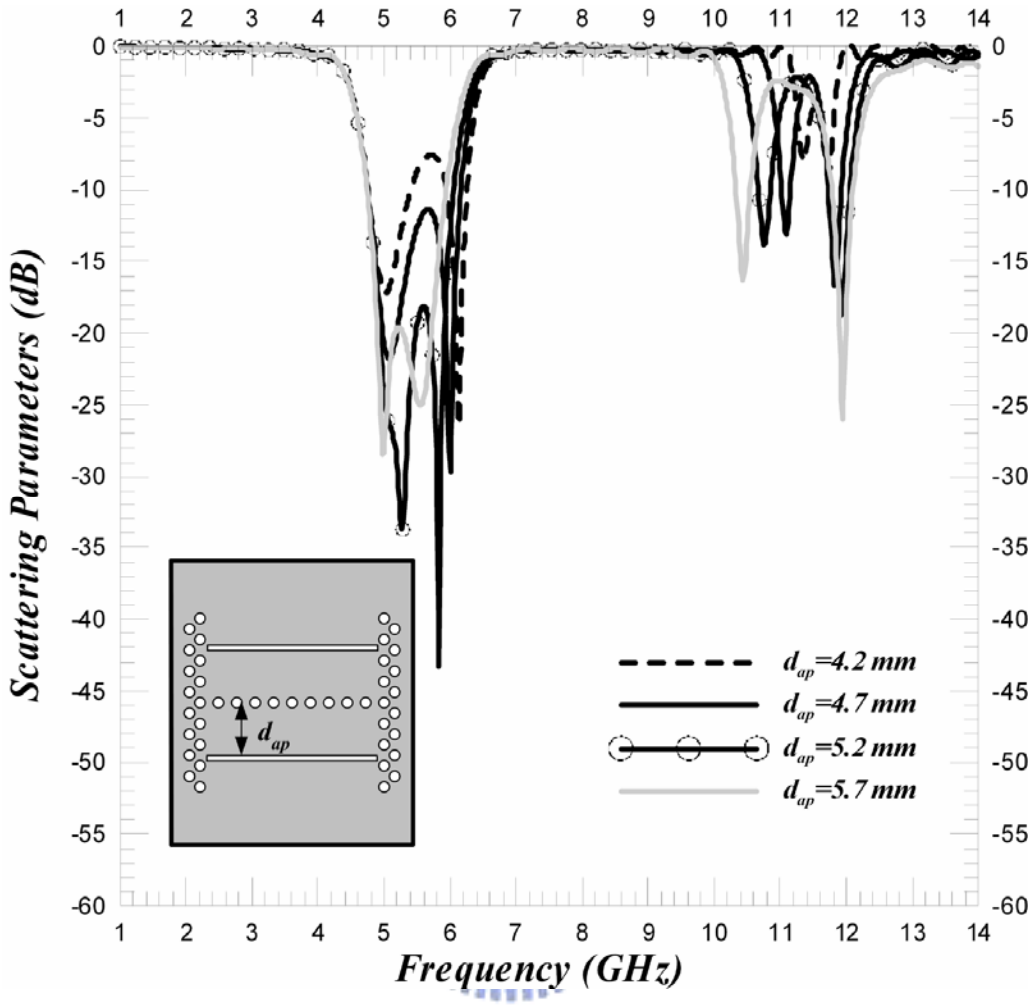
Scattering Parameters (dB)
Frequency (GHz)
d_{ap}
d_{ap}=4.2 mm
d_{ap}=4.7 mm
d_{ap}=5.2 mm
d_{ap}=5.7 mm

Fig. 4.4 (a)

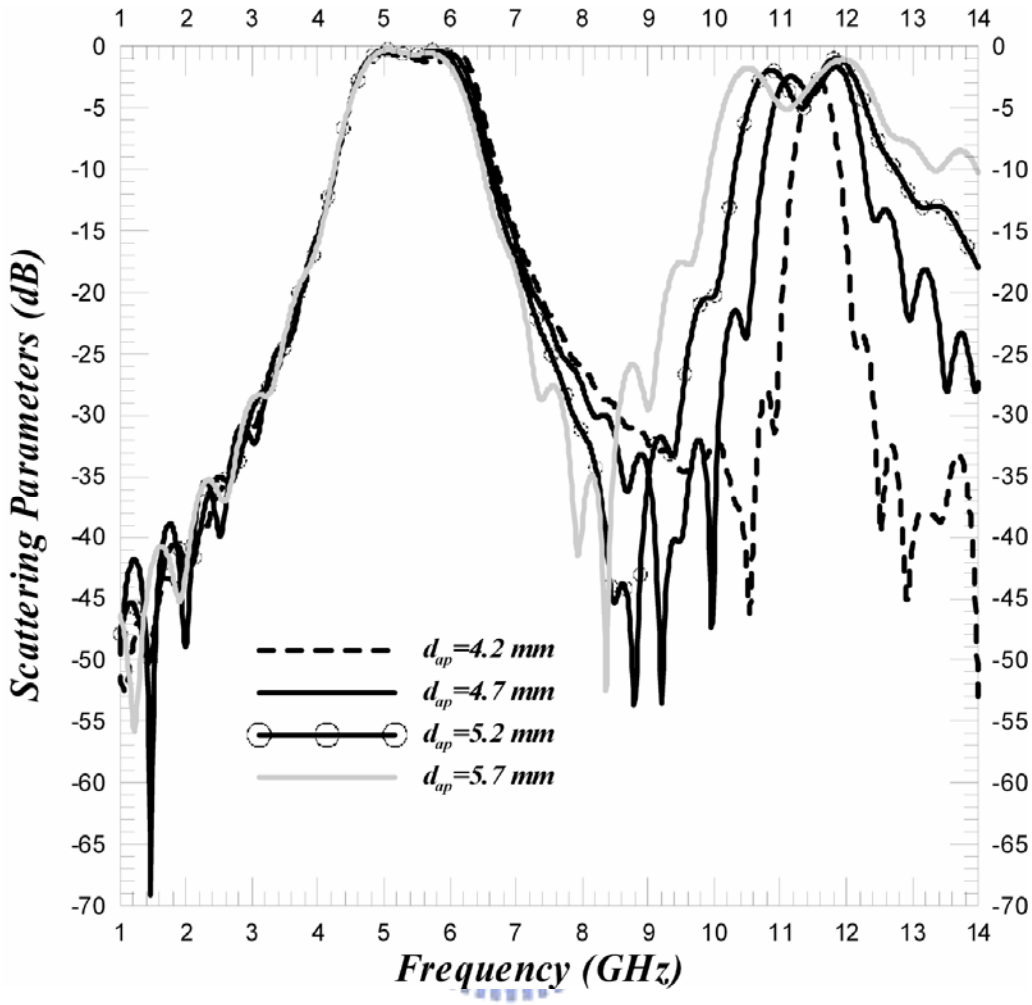

Fig. 4.4 (b)

Figure 4.4 The simulation of the tunable band-pass filter with the distance of aperture

(a) return loss (b) insertion loss

As shown in Figure 4.5 (a)-(d), the band-pass filter is designed, fabricated on a standard PCB process using via-hole-wall. The Figure 4.6 shows that photo of the proposed band-pass filter which combined first layer with second layer with screw.

Figure 4.7 depicted the measured and simulated results for the insertion and return loss of the band-pass filter. The two coupling apertures share the same width and length, which are 0.6 mm and 17 mm, respectively. The length, width and thickness of the resonance cavity are 15 mm, 17 mm and 0.508 mm, respectively. The dashed lines denote the measured result, while the solid lines represent the simulated result. The band-pass filter exhibits an insertion loss about -1.59 dB, which is slightly higher than simulated value of -0.47dB, and a return loss <-10.3 dB compared to a simulated value <-16.6dB over the pass-band shown in Figure 4.7. The measured results give a 3-dB bandwidth of 36.8% at a center frequency of 5.4GHz. Since the thickness of the cavity is far smaller than the width and length, the major component of the electric field in the cavity is E_z, while the E_x and E_y are negligible. Therefore, the lowest resonant mode is TM_{110} in this example. The resonant frequency for the (m, n, o) mode of the cavity without apertures is given below

$$f(in \quad GHz) = 150\sqrt{(m/w)^2 + (n/l)^2} \,/\, \sqrt{\varepsilon_s} \qquad (4.2)$$

Where the integer m and n denote the index number along width and length direction, respectively. We use equation (4.2) to obtain the resonant frequency is about 6.44 GHz. The relative dielectric constant of the substrate is characterized by ε_s. However, due to the existence of two coupling apertures, the resonance frequency should be different with the value given in (4.2). From Figure 4.7, it is obvious to see that the excellent agreement between the simulated and measured results.

As mentioned earlier, the band-pass characteristics of this filter is based on the resonance effect of the cavity. To prove that the band-pass characteristic is due to the resonant mode, TM_{110}, we plot the contour map, depicted in Figure 4.8, for the vertical component of electric field strength (E_z) on the cross section at z=0.5h (h is the thickness of the substrate) at the resonant frequency (5.4GHz). Form this figure, it is apparently to see that the maximum electric field is around the center of the cavity and the field variation resembles the function given below.

$$E_z(x,y) \approx \sin\frac{\pi x}{w_x}\sin\frac{\pi y}{w_y} \tag{4.3}$$

It is clearly observed that double rows of via-wall are sufficient to block the electromagnetic field leakage through the vias.

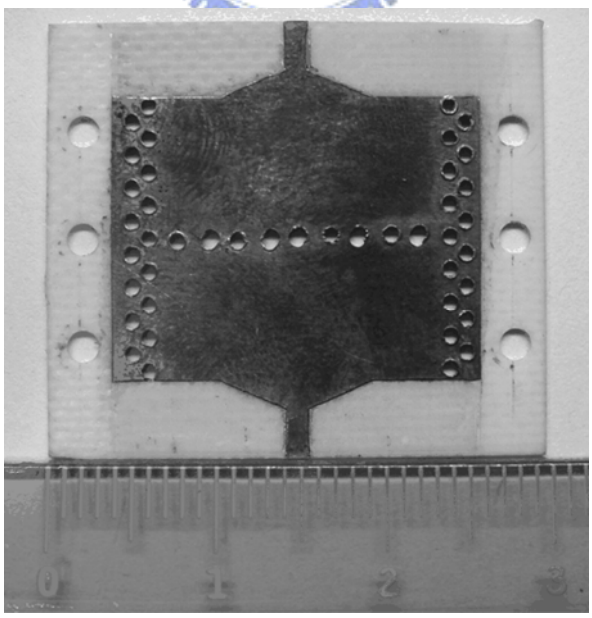

Fig. 4.5 (a)

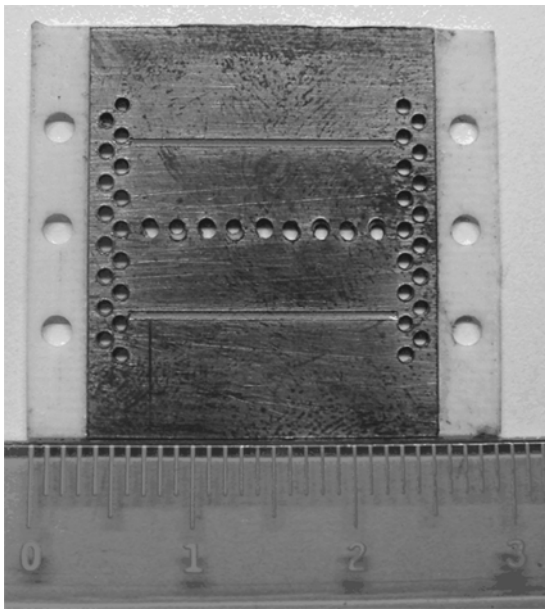

Fig. 4.5 (b)

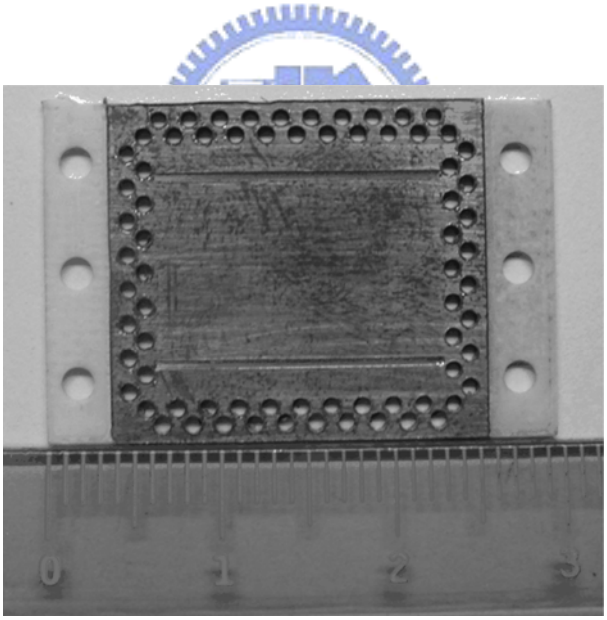

Fig. 4.5 (c)

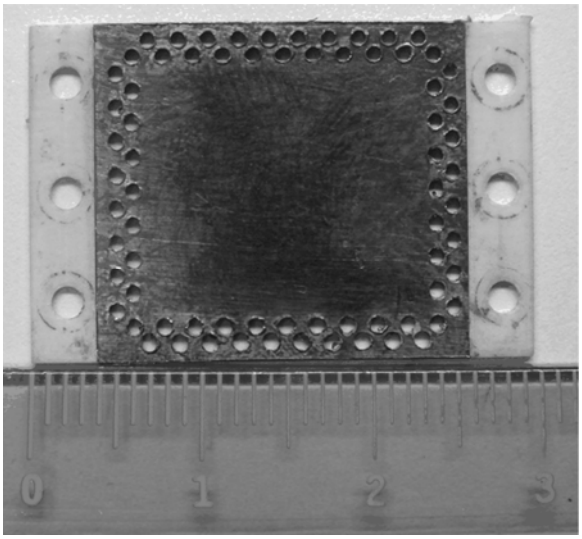

Fig. 4.5 (d)

Figure 4.5 The layout of the band-pass filter (a) top view of the first layer (b) bottom view (c) top view of the second layer (d) bottom view showing the resonant cavity.

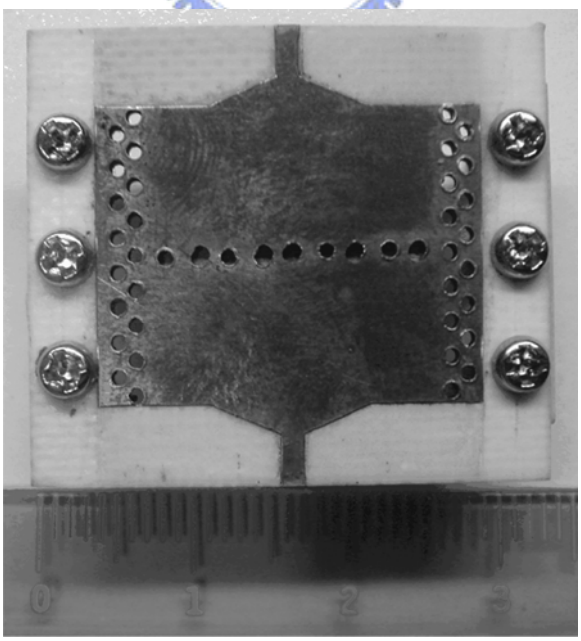

Fig. 4.6 (a)

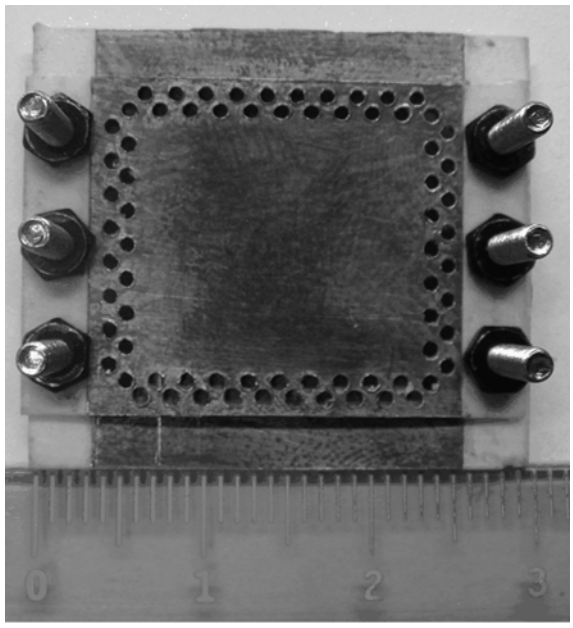

Fig. 4.6 (b)

Figure 4.6 Photo of the proposed band-pass filter.(a) top view (b) bottom view.

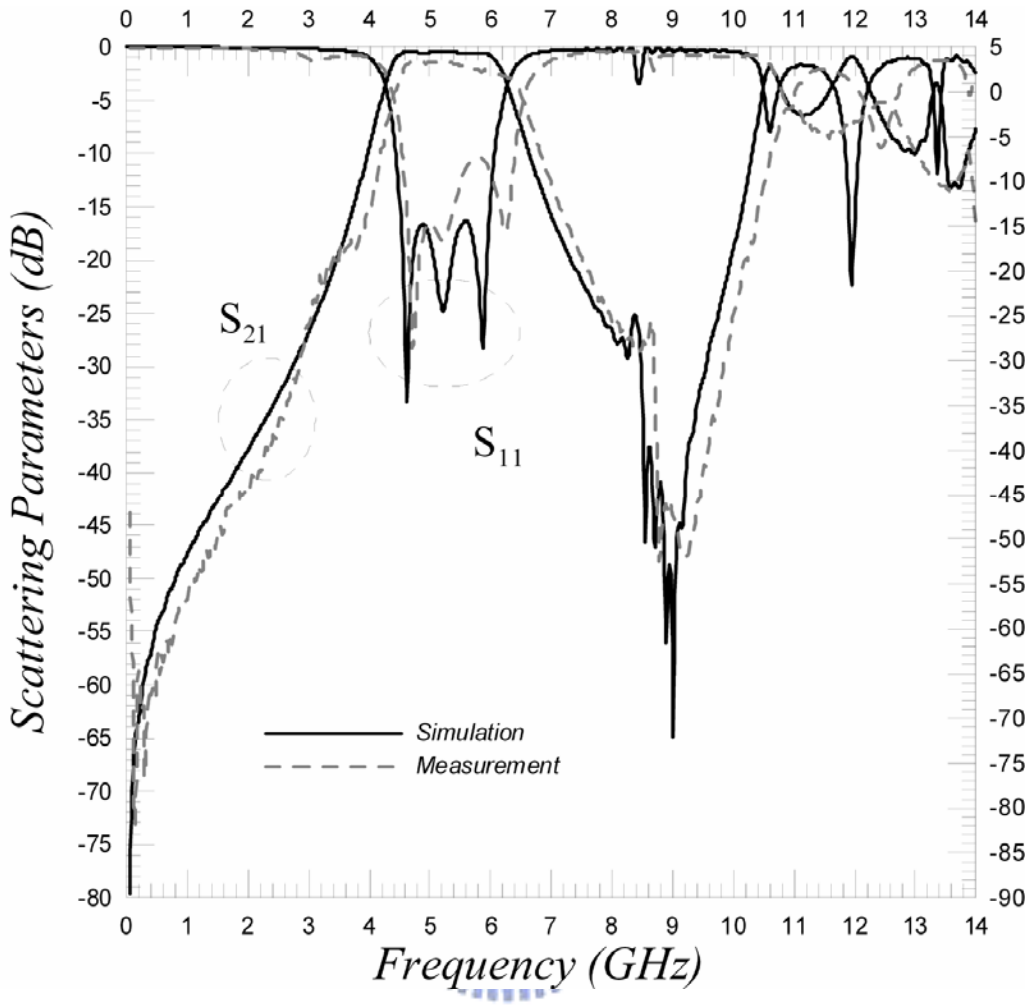

Figure 4.7 measured and simulated insertion and return loss for the band-pass filter with aperture length 17 mm.

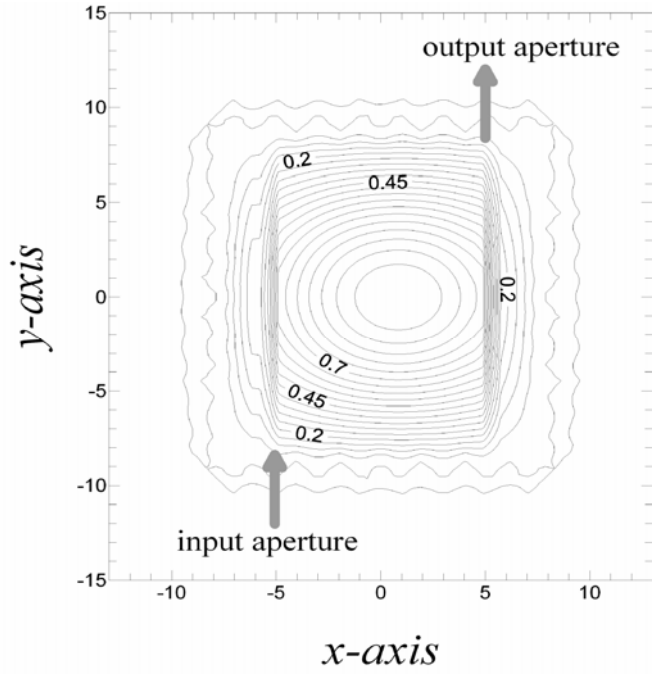

Figure 4.8 Distribution of the field contour (E_z component) inside the resonant cavity over the cross section at the position z =0.5h, where h is the thickness of the substrate.

In the following two examples, we change the aperture length while keeping all the other parameters given in the previous example. The lengths of the aperture are 15 mm and 13 mm in Figure 4.9 and 4.10. Comparing Figure 4.9 and 4.10 with Figure 4.7, it is apparently to see that the bandwidth is decreasing as the aperture length is decreased. It is noted that the insertion loss in Figure 4.10 increases, compared with those in Figure 4.7 and 4.9. It may be conjectured that due to the decrease in the length of coupling aperture the coupling coefficient between the waveguide and cavity decreases accordingly. The bandwidth of the three cases shown in Figure 4.7, 4.9 , 4.10 and 4.11 are 36.8%, 32.9%, 31.3% and 12.8%, respectively. Figure 4.10 show that insertion loss about -2dB was larger than the insertion loss of the aperture length 17mm and 15mm. We found that the bandwidth decreases as the decrease in the

aperture length, however, the insertion loss increases. We have also carried out the numerical simulations and experimental studies for the cases with several different aperture lengths.

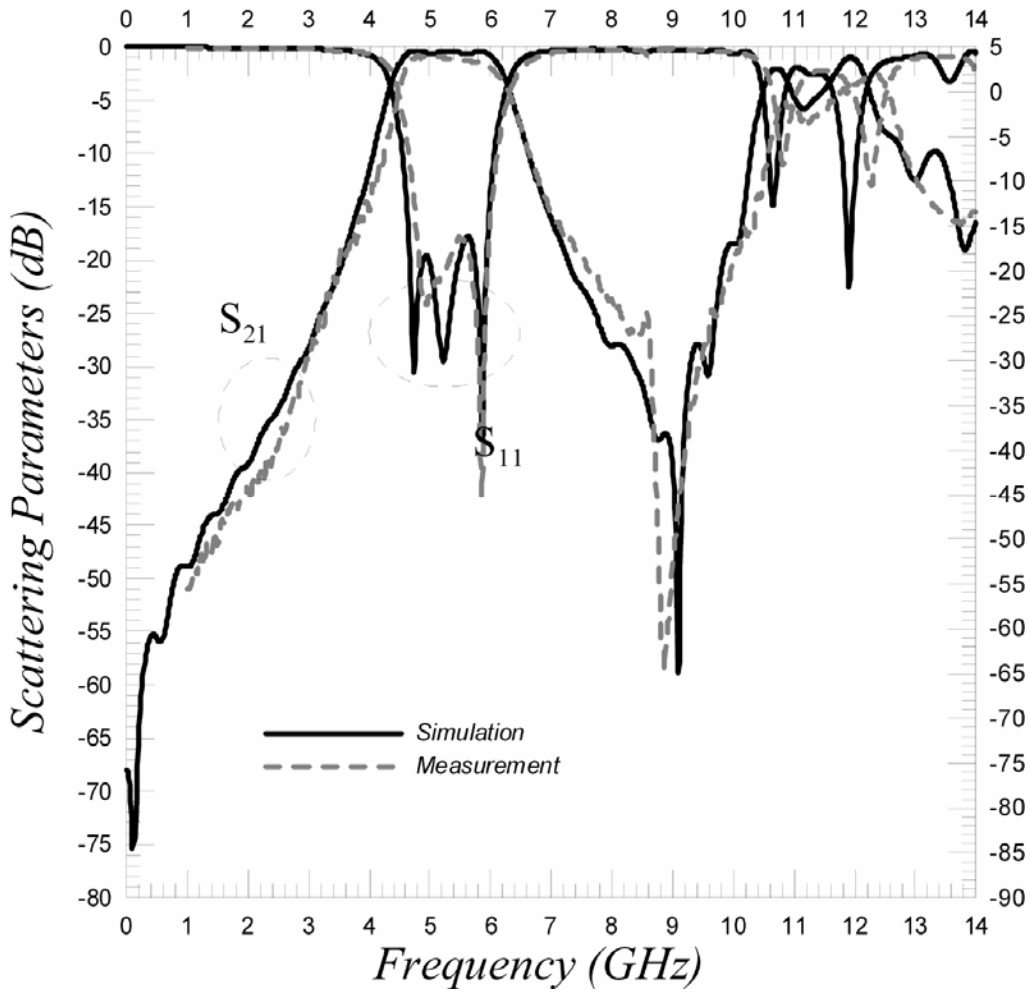

Figure 4.9 Measured and simulated insertion and return loss for the band-pass filter with aperture length 15mm.

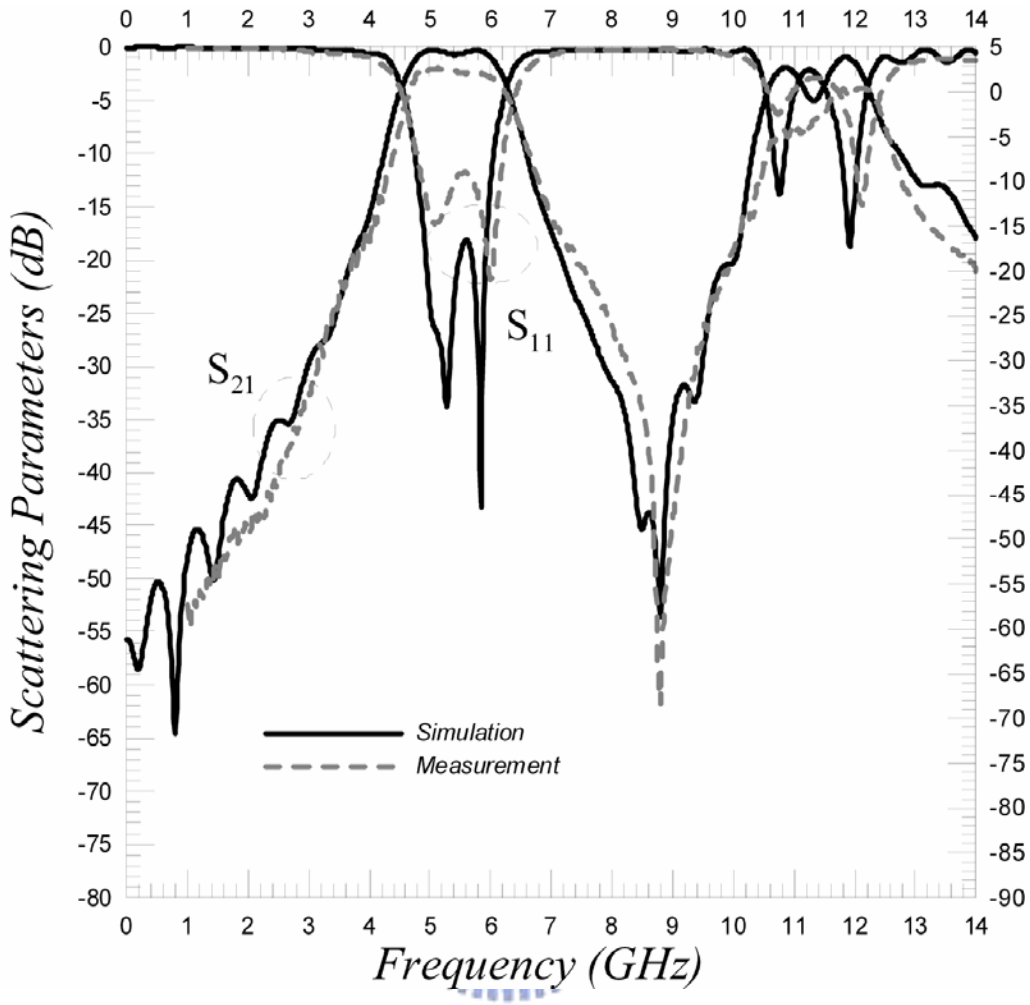

Figure 4.10 Measured and simulated insertion and return loss for the band-pass filter with aperture length 13mm.

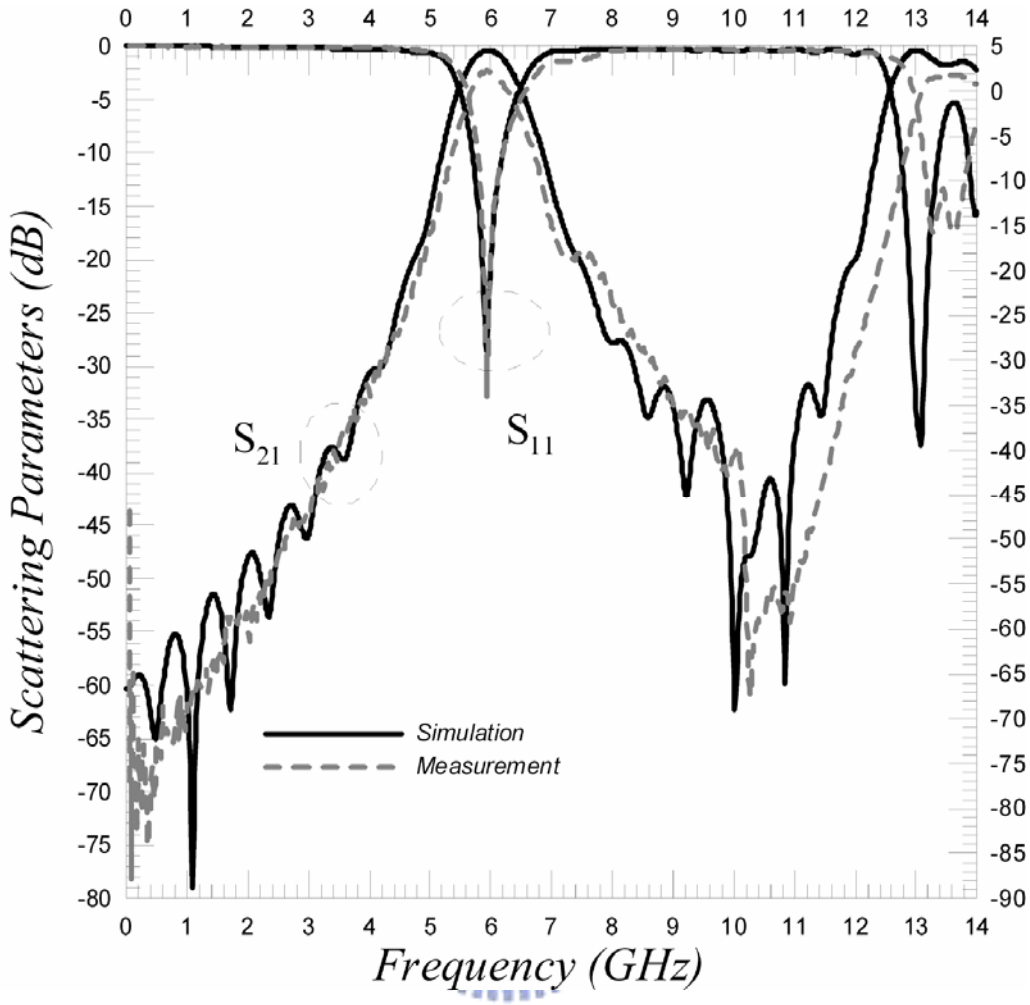

Figure 4.11 Measured and simulated insertion and return loss for the band-pass filter with aperture length 8mm.

Chapter 5

Conclusion

A novel band-pass filter using a resonant cavity based on the via-hole-wall technology has been developed. The pass-band frequency can be estimated by the resonant frequencies of the cavity. Besides, the bandwidth of this band-pass filter can be altered by turning the length of coupling aperture. Due to the vertical coupling between the substrate integrated waveguide and cavity, the size of the structure is further reduced. Measured and simulated results using CST Microwave Studio have been presented and discuss. A good agreement between the measured and simulation results was obtained. Such types of filter are valuable in the design and realization of low-cost microwave and millimeter wave system.

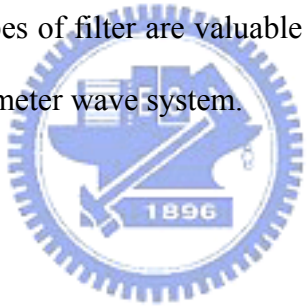

Reference

[1] Jong-Hoon Lee, Stephane Pinel, John Papapolymerou, Joy Laskar and Manos M. Tentzeris, “ Low-loss LTCC cavity filters using system -on-package technology at 60 GHz ” IEEE Trans. Microw. Theory Tech., vol. 53, no. 12, pp.3817-3824, December, 2005

[2]H. J. Hsu, M. J. Hill, J. Papaolymerou, and R. W. Ziolkowski, “ A planar X-band electromagnetic bandgap (EBG) 3-pole filter,” IEEE Microw. Wireless Compon. Lett., vol. 12, no. 7, pp. 255-257, Jul. 2002.

[3]W. Chappell, M. Little, and L. Katehi, “High isolation, planar filters using EBG substrates.” IEEE Microwave Wireless Compon. Lett., vol. 11, pp. 246-248, June 2001.

[4] M. J. Hill, R. W. Ziolkowski, and J. Papapolymerou, “Simulated and measured results from a Duroid-based planar MBG cavity resonator filter,” IEEE Microw. Wireless Compon. Lett. vol. 10, no. 12, pp.528-530, Dec. 2000.

[5]C. A. Tavernier, R. M. Henderson, and J. Papapolymerou, “A reduced- size silicon micromachined high-Q resonator at 5.7GHz,” IEEE Trans. Microw. Theory Tech., vol. 50, no. 10, pp. 2305-2314, Oct. 2002.

[6]Yu Lin Zhang, Wei Hong, Ke Wu, Ji Xin, Chen and Hong Jun Tang, “Novel Substrate Integrated Waveguide Cavity Filter with Defected Ground Structure,” IEEE Trans. Microw. Theory Tech., vol 53, no. 4, pp. 1280-1287, April. 2005.

[7]Y. Cassivi and K. Wu,”Low cost microwave oscillator using substrate integrated waveguide cavity,” IEEE Microw. Wireless Compon. Lett., vol. 13, no. 2, pp. 48-50, F eb. 2003.

[8]Yu Lin Zhang, Wei Hong, Ke Wu, Ji Xin, Chen and Zhang Cheng Hao,

"Development of compact bandpass filters with SIW triangular cavities," Microwave Conference Proceedings, 2005. APMC 2005. Asia-Pacific Conference Proceedings, Volume 1, Issue , 4-7 Dec. 2005 Page(s): 4 pp.,

[9]Z. C. Hao, W. Hong, X. P. Chen, J. X. Chen, K. Wu, and T. J. Cui, "Multilayered substrate integrated waveguide (MSUBSTRATE INTEGRATED WAVEGUIDE) elliptic filter," IEEE Microw. Wireless Compon. Lett., vol. 15, no. 2,pp. 95-97, Feb. 2005.

[10]Feng Xu and Ke Wu, "Guided-Wave and Leakage Characteristics of Substrate Integrated Waveguide," IEEE Trans. Microw. Theory Tech., vol. 53, no. 1, pp. 66-73, Jan. 2005.

[11]Y.Cassivi, L. Perregrini, P. Arcioni, M. Bressan, K. Wu, and G. Conciauro, "Dispersion characteristics of substrate integrated rectangular waveguide," in IEEE Microwave Wireless Compon. Lett., vol. 12, Sep. 2002, pp. 333-335.

[12]D. Deslandes and K. Wu. "Single-substrate integration techniques for planar circuits and waveguide filters", IEEE Transactions on Microwave Theory and Techniques, Feb. 2003, pp. 593-596.

[13]D. Deslandes and K. Wu. "Design consideration and performance analysis of substrate integrated waveguide components", Milano, European Microwave Conference, 23-27. Sept. 2002. pp. 881-884.

[14]R. E. Collin, Foundations for Microwave Engineering. New York: Mc-Graw-Hill, 1992.

[15]D. M. Pozar, Microwave Engineering, 2ed. New York: Wiley, 1998.